Nuclear Instruments and Methods in Physics Research B 557 (2024) 165543

Contents lists available at ScienceDirect

Nuclear Inst. and Methods in Physics Research, B

journal homepage: www.elsevier.com/locate/nimb

Measurements of displacement cross sections of metals for 120-GeV proton beam irradiation

Yosuke Iwamoto [a,*], Hiroki Matsuda [b], Shin-ichiro Meigo [c], Katsuya Yonehara [d], Frederique Pellemoine [d], Zunping Liu [d], Kevin Lynch [d], Makoto Yoshida [e], Atsushi Yabuuchi [f], Toshimasa Yoshiie [g], Shintaro Hashimoto [a]

[a] Japan Atomic Energy Agency, Nuclear Science and Engineering Center, Tokai, Naka, Ibaraki 319-1195, Japan
[b] National Institutes for Quantum Science and Technology, Institute for Advanced Synchrotron Light Source, Aoba, Sendai, Miyagi 980-8579, Japan
[c] Japan Atomic Energy Agency, J-PARC Center, Tokai, Naka, Ibaraki 319-1195, Japan
[d] Fermi National Accelerator Laboratory, Batavia IL 60510-5011, USA
[e] High Energy Accelerator Research Organization (KEK), Tsukuba, Ibaraki 305-0801, Japan
[f] Kyoto University, Institute for Integrated Radiation and Nuclear Science, Asashiro-Nishi, Kumatori, Sennan, Osaka 590-0494, Japan
[g] Osaka Metropolitan University, Graduate School of Engineering, Sumiyoshi-ku, Osaka, Japan

ARTICLE INFO

Keywords:
Displacement damage
Proton
Accelerator
DPA
Metal

ABSTRACT

The number of displacements per atom (dpa) is widely used as an indicator of irradiation damage of materials in proton accelerator facilities. Experiments have been carried out to validate the dpa of metallic materials for protons with energies below 3 GeV. However, measurements of the displacement cross-sections for high-energy protons above 3 GeV have not been carried out and the calculations have not been validated. To validate the displacement cross section of metals in high-energy region, electrical resistivity changes in wires of aluminum, copper and tungsten at 8 K were measured using protons with energies of 120-GeV. The results show that the Norgett-Robinson-Torrens dpa model of the Particle and Heavy Ion Transport Calculation Code overestimates the experimental data. On the other hand, the calculated results using the athermal recombination corrected dpa model were in agreement with the measured displacement cross sections. In the proton energy region above 1 GeV, the displacement cross section is almost constant, which is due to the fact that the damage energy of the material under 1 GeV proton irradiation is almost the same as under 120 GeV proton irradiation. Damage recovery of defects accumulated in the sample was also measured using isochronal annealing: At 80 K, approximately 60 % and 80 % of the damage remains for copper and tungsten, respectively. These results are the same as those obtained from other experiments on proton and neutron irradiation.

1. Introduction

High-intensity proton accelerator facilities at the Japan Proton Accelerator Research Complex (J-PARC) [1], the Fermi National Accelerator Laboratory (FNAL) [2], the European Organization for Nuclear Research (CERN) [3] and elsewhere provide new means of research using a wide variety of secondary particles and contribute to research and development in a wide range of fields from fundamental physics to industrial applications. The beam power of these accelerator facilities is limited by the viability of the production targets and beam windows. It is recognized that the most important cross-cutting issue for high power target facilities is radiation damage to component materials. Damage assessment of materials is essential for the reliable operation of high-power accelerators.

The displacement per atom (dpa) value is widely used for the lifetime estimation of materials at proton accelerator facilities with Monte Carlo (MC) particle transport codes. In MC codes, the Norgertt-Robinson-Torrens (NRT) model is employed to calculate the number of Frenkel pairs (NRT-dpa) [4]. Molecular dynamics (MD) simulations [5], on the other hand, have been in use for the last two decades for the study of defect formation in a wide variety of materials. As an example, Nordlund et al. used MD simulations to account for real-world displacement damage and reported the athermal recombination correction (arc) in which many Frenkel pairs in the metal recombine in 10^{-10} s [5].

* Corresponding author.
E-mail address: iwamoto.yosuke@jaea.go.jp (Y. Iwamoto).

https://doi.org/10.1016/j.nimb.2024.165543
Received 27 May 2024; Received in revised form 7 September 2024; Accepted 8 October 2024
Available online 16 October 2024

For the validation of dpa calculations with MC codes, it is necessary to measure the electrical resistivity change at cryogenic temperature where the thermal motion of Frenkel pairs is frozen. The displacement cross section is the probability that an irradiated particle will displace an atom of material, and the value of dpa is the product of the fluence of the irradiated particle and the displacement cross section. We have measured the displacement cross sections of various metals (aluminum, copper, and tungsten) under proton irradiation of 100 MeV ~ 3 GeV energy using our cryogenic irradiation chamber [6–9].

Comparing the experimental and calculated results, the arc-dpa values agreed well with the experimental values, while the NRT-dpa values were about three times larger than the experimental values in the proton energy range of 100 MeV-3 GeV. In contrast, no experimental data for incident protons with energies over 3 GeV are available. The FNAL-led Radiation Damage In Accelerator Target Environments (RaDIATE) collaboration supports advances in particle physics by identifying ways to mitigate radiation damage to accelerator materials, with the aim of significantly increasing beam power in the future [10]. This collaboration recognizes the importance of displacement cross section measurements for the assessment of radiation damage to materials in accelerator facilities. In particular, experimental data are essential to validate the assessment of damage to materials for 3 GeV-400 GeV proton beams at J-PARC, FNAL and CERN, which are required for neutrino physics experiments.

In this study, for the validation of dpa calculations for high-energy proton irradiation over 3 GeV, displacement cross sections of aluminum, copper and tungsten under 120 GeV proton irradiation were measured at the Fermi Accelerator Test Beam Facility (FTBF) [11]. The experimental results were compared with computational results with the Particle and Heavy Ion Transport code Systems (PHITS) [12]. Isochronal annealing was also performed to measure the amount of recovery of accumulated defects in the sample.

2. Methods

This section indicates experimental and calculation methods to obtain the displacement cross section based on our previous papers [6–9].

2.1. Experimental methods

The experimental displacement cross section, σ_{exp} [m^2], is determined by measuring the increase in electrical resistivity, $\Delta\rho_{\mathrm{m}}$ [Ωm], of the sample due to beam irradiation at cryogenic temperatures, using the following formula:

$$\sigma_{exp} = \frac{1}{\rho_{FP}}\frac{\Delta\rho_m}{\phi} = \frac{1}{\rho_{FP}}\frac{A}{L}\frac{\Delta R}{\phi} \quad (1)$$

where A/L is the geometry factor of the sample. L [m] is the length between both potentials of the wire. A [m] is the wire cross-sectional area. ϕ [1/m^2] is the incident proton fluence on the target. ΔR [Ω] is the changes in electrical resistances of the wire. Table 1 lists the variation of resistivity per density of Frenkel-pair for selected metals, ρ_{FP}, [13] adopted in this study. In the experiment, $\Delta\rho_{\mathrm{m}}$ and ϕ were measured to obtain the experimental displacement cross section.

The measurement was performed in the M03 tunnel at FTBF. Fig. 1 shows the arrangement of the experimental apparatus.

The 120 GeV proton beam with a spill time of 4.2 sec every 60 sec was irradiated onto the sample wire in the target chamber. The beam intensity was about 1.8×10^{11} protons per spill. For beam scanning, a Segmented Wire Ionization Chamber (SWIC) was installed at the rear of the target chamber. A helium gas compressor to operate the cryocooler and a data aquation system were located approximately 15 m from the target chamber. The target chamber developed in our previous study [8] was placed on a moving table in the beamline. Fig. 2 shows the target chamber with the air-cooled Gifford-McMahon (GM) refrigerator (RDK-408D2, Sumitomo Heavy Industries, Ltd.). To prevent thermal radiation to a sample assembly in the target chamber, a sample assembly was covered with a 1 mm thick aluminum plate. A 0.5 mm thick titanium window is used in the target chamber beam window as a vacuum barrier.

Fig. 2 also shows the sample assembly. Sample wires were placed on the insulator tape made of Kapoton® on the aluminum plates with an aperture of 50 mm to avoid beam interaction on the plate. Four different wire samples (aluminium, copper, niobium and tungsten) with a diameter of 0.25 mm purchased from Niraco were used in the experiments. Note that this study did not employ experimental data using niobium wire, the reasons for which are explained in the following paragraphs.

Table 2 lists the properties of the wire samples for aluminum, copper, and tungsten. To measure the temperature on the plate, a calibrated Cernox resistance thermometer (CX1050-CU-HT) was mounted on an aluminum plate. A 24 Ω resistance electric heater was mounted on a copper block and current generated by a Lakeshore Model 335 cryogenic controller was passed through the heater to heat the wire sample and aluminum plate. The recovery of accumulated defects by isochronous annealing after irradiation was investigated using an electric heater. The temperature of the aluminum plate was 4 K after cooling the samples at room temperature for 6 h. Note that a niobium wire was also attached to the aluminum plate. The electrical resistance of niobium at 4 K was 10^{-8} Ω due to its superconducting state. The temperature of the aluminum plate was set at 8 K by an electric heater to avoid the superconducting state of niobium wire. In this work, the experimental data for niobium have not been reported in this paper due to the unexpected increase in electrical resistance during proton irradiation. The results for niobium will be discussed in another paper.

To reduce defects in the wires prior to irradiation, aluminum (melting point 933.5 K) and copper (melting point 1358 K) were annealed using a vacuum electric furnace capable of heating to 1500 K, and tungsten (melting point 3695 K) was annealed using an electron gun capable of heating to about 2500 K. For aluminum and copper, the annealing temperatures were set so that the ratio between annealing temperature and melting point was 0.9–0.95. For tungsten, the annealing temperature was set at 2473 K, taking into account an electron gun heating limit of 2500 K.

The data acquisition system for measurement of the electrical resistance is shown in Fig. 3. A current source (6221, Keithley Instruments) in combination with a nanovoltmeter (2182A, the same company) measured the electrical resistance for the sample wire. The principle of operation is the application of pulses of opposite polarity and the measurement of the voltage during each pulse. The effect of thermal electromotive force can be cancelled out by taking the difference between the measured values of the positive and negative pulses [14]. Table 2 also shows the length between the two potential points on the wire sample. DAQ6510 and 7700 20-channel multiplexers were used to switch the electrical signals of the four samples sequentially to the current source and nanovoltmeter. As shown in Fig. 2, a Lakeshore Model 335 cryogenic temperature controller was used to collect signals from a Cernox resistance thermometer and a 24 Ω electric heater. All signals were sent to a laptop. A data acquisition program was written in Labview.

Table 1
Variation of resistivity per density of Frenkel-pair for selected metals [13] adopted in this study.

Material	Aluminum	Copper	Tungsten
Adopetd ρ_{FP} [μΩm]	3.7 ± 0.6	2.2 ± 0.5	27 ± 6

2.2. Calculation methods in PHITS

The damage energies which are characteristic of the displacement

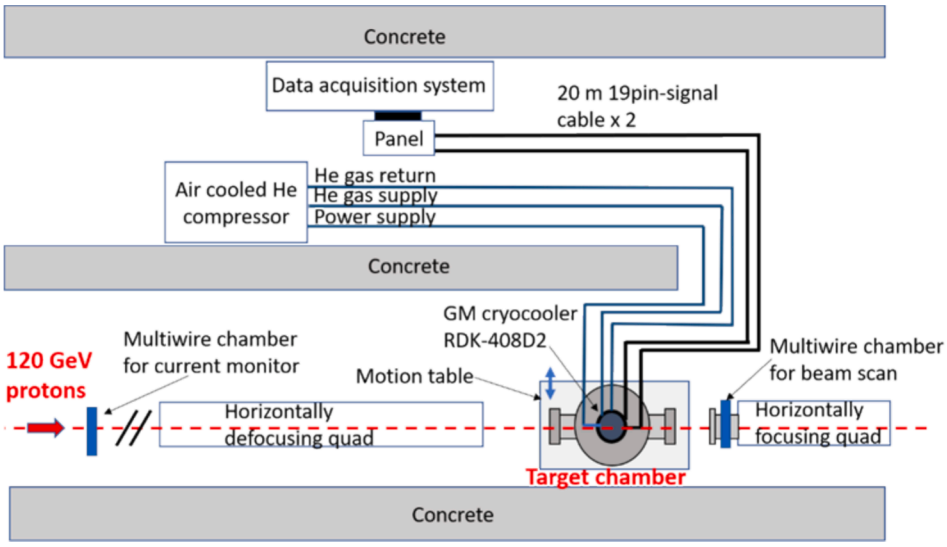

Fig. 1. Arrangement of the experimental apparatus. in the M03 tunnel at FTBF.

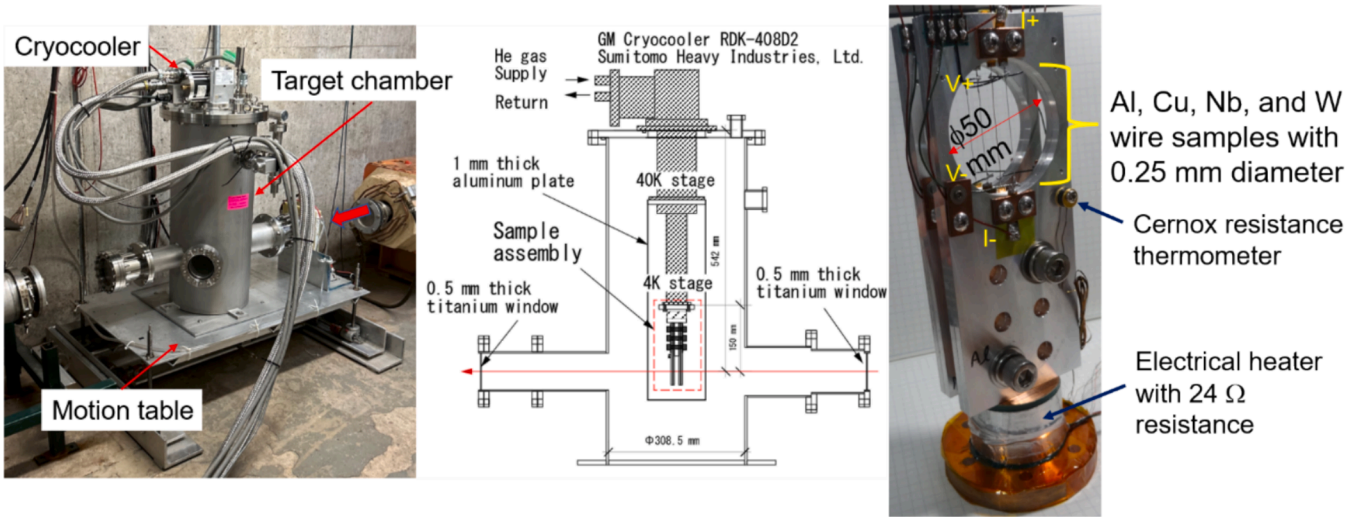

Fig. 2. Target chamber with GM cryocooler (left and center sides) and the sample assembly (right side).

Table 2
Properties of wire samples, including the length between two potential points, and geometry factor which is the ratio of wire cross sectional area to length between two potential points.

Material	Aluminum	Copper	Tungsten
Purity [%]	99.99	99.999	99.95
Melting point [K]	933.5	1358	3695
Annealing temperature [K]	840	1289	2473
Annealing time [minute]	30	30	15
Diameter [mm]	0.25	0.25	0.25
Length between two potential points [mm]	40	37.5	37.5
Geometry factor [m]	1.23×10^{-6}	1.31×10^{-6}	1.31×10^{-6}

cascade are used for the description of the different irradiation conditions. The damage energy is the energy that is available to produce a displacement of atoms by means of elastic collisions. Fig. 4 shows the method used to calculate dpa in arbitrary geometry with the [t-dpa] tally in PHITS. The incident particle generates primary knock-on atoms (PKA) by Coulomb scattering until a nuclear reaction occurs, which leads to defects. Secondary charged particles produced by the nuclear reaction between the incident particle and the target nucleus also generate PKA by Coulomb scattering, which leads to defects. This flow is repeated in MC simulation with the number of trials and the averaged dpa values in a region are calculated. Details of the calculation methods are described in our previous paper [15,16]. The main features of the calculation are described as follows.

The projectile and the secondary particles produce PKA in the target material. The damage energy to the target material during Coulomb scattering by the incident and secondary particles is proportional to PKA production. When neutral particles such as neutrons are produced, the charged particle produced by the nuclear reaction between the neutral particle and the target nucleus is considered PKA.

The damage energy depends on the kinetic energy of the particles, especially the kinetic energy of the secondary particles, which is determined by the nuclear reaction between the incident particles and the matter. In PHITS, nuclear reactions are described using INCL4.6 [17] and the Jet AA Microscopic transportation Model, JAM [18], in the respective energy regions. When the residual nuclei with excitation energies are calculated by these methods, the de-excitation process of the residual nuclei is described by the Generalized Evaporation Model

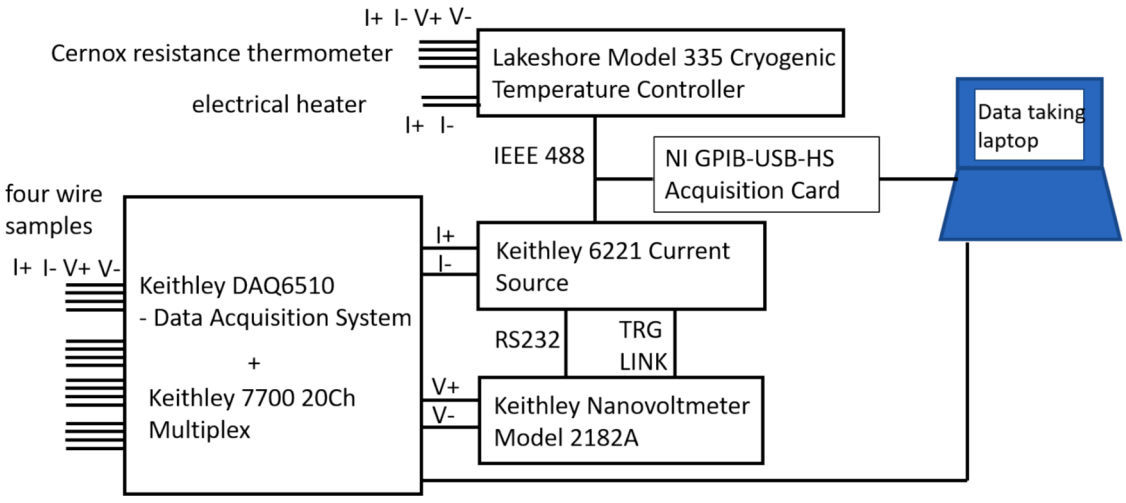

Fig. 3. Data acquisition system for measurement of the electrical resistance.

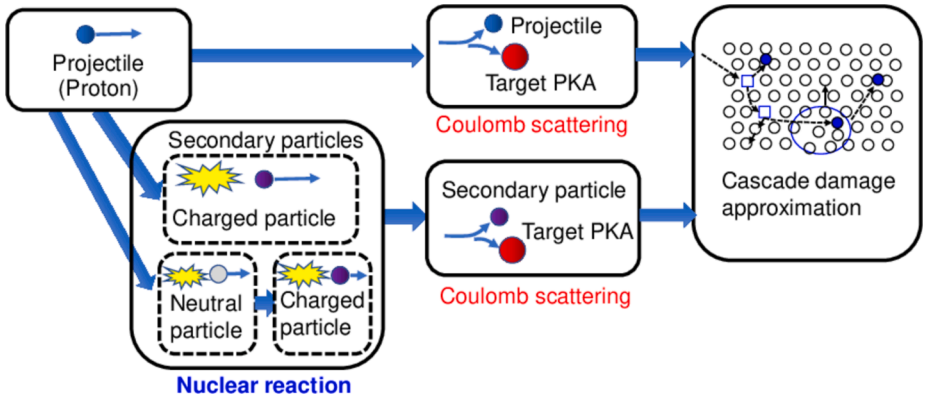

Fig. 4. Method used to calculate dpa in arbitrary geometry with the [t-dpa] tally in PHITS.

GEM [19]. The calculations using these nuclear reaction models give the type and number of secondary particles and the kinetic energy of each.

The NRT model, as a function of the damage energy, T_d, gives the number of production defects in the irradiated material, ν_{NRT}, as:

$$\nu_{NRT}(T_d) = \begin{cases} 0, T_d < E_d \\ 1, E_d < T_d < \dfrac{2E_d}{0.8} \\ \dfrac{0.8T_d}{2E_d}, \dfrac{2E_d}{0.8} < T_d \end{cases} \quad (2)$$

where E_d is the averaged displacement energy of a target atom. Fig. 5 shows the damage energy relative to the PKA energy, T, during the self-irradiation [20]. In the low PKA energy region, there is energy loss due to elastic collision and there is no electronic excitation, therefore the damage energy increases linearly with increasing PKA energy. In the high PKA energy region, the energy loss due to electronic excitation, which does not contribute to displacement damage, increases with PKA energies, while the energy loss due to elastic collisions remains constant. The damage energy is therefore constant in the high PKA energy region. Furthermore, when inelastic collisions occur in the high PKA energy region, the secondary particles produced contribute to displacement damage through elastic collisions.

The average NRT-dpa per incident proton in a target region, DPA_{NRT}, is calculated by the MC method on the basis of the following equations for summing over delivered protons, N_p:

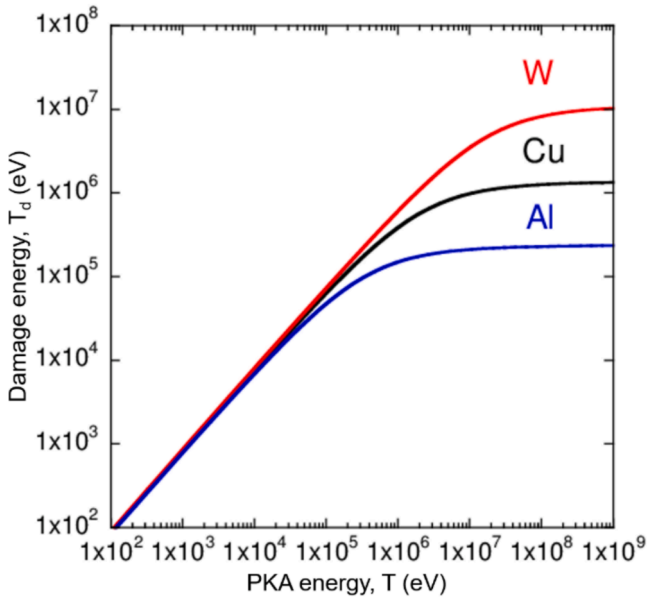

Fig. 5. Damage energy, T_d, relative to the PKA energy, T, during the self-ion irradiation [20].

$$DPA_{NRT} = \frac{1}{N_t \times V_t \times N_p} \times \sum_i^n l_i \times \int_{t_d}^{t_{max,i}} \frac{d\sigma_{Coul}}{dt_i} \nu_{NRT}(T_d) dt_i, \quad (3)$$

where t_i is the dimensionless collision parameter of an ith charged particle including the transferred energy, T_d, to target atom [21]. t_d is the dimensionless collision parameter corresponding to the displacement threshold energy, E_d, and $t_{max,i}$ is the maximum dimensionless collision parameter of an ith charged particle. N_t is the target atom density and V_t is the volume of a target region. n is the total number of charged particles. l_i is the travel distance of an ith charged particle in a target. $\frac{d\sigma_{Coul}}{dt}$ is a universal one-parameter differential scattering cross section equation with a function of a dimensionless collision parameter t [21]. For the calculated displacement cross section, σ_{NRT} is obtained from the following equation:

$$\sigma_{NRT} = \frac{DPA_{NRT}}{\phi_p}, \quad (4)$$

where ϕ_p is the particle fluence of the projectile. The energy deposition to the target is negligible for 120-GeV proton.

The arc model with the defect production efficiency, including the effect of Frenkel pair recombination, has been applied to the NRT-dpa with the following equation:

$$\xi_{arc}(T_d) = \frac{1-c}{(2E_d/0.8)^b} T_d^b + c, \quad (5)$$

where b and c are the material constants as determined by MD simulations [5,22]. The material parameters for b, c and the threshold displacement energy E_d are given in Table 3.

The number of displacements calculated with NRT model in **Eqs. (2), 3,** and **4** are replaced with the following:

$$\nu_{arc}(T_d) = \begin{cases} 0, T_d < E_d \\ 1, E_d < T_d < \frac{2E_d}{0.8} \\ \frac{0.8T_d}{2E_d}\xi_{arc}(T_d), \frac{2E_d}{0.8} < T_d \end{cases}, \quad (6)$$

$$DPA_{arc} = \frac{1}{N_t \times V_t \times N_p} \times \sum_i^n l_i \times \int_{t_d}^{t_{max,i}} \frac{d\sigma_{Coul}}{dt_i} \nu_{arc}(T_d) dt_i, \quad (7)$$

$$\sigma_{arc} = \frac{DPA_{arc}}{\phi_p}, \quad (8)$$

Previous measurements of the displacement cross section using protons with energies below 3 GeV have shown that arc-dpa, which takes recombination corrections into account, reproduces the experimental data well, while conventional NRT-dpa, which does not include recombination corrections, overestimates the experimental data.

3. Results

This section describes the experimental displacement cross section including electrical resistance change during 120 GeV proton beam irradiation. Experimental results on the recovery of point defects by annealing with an electric heater after beam irradiation are also discussed.

Table 3
Material parameters for b, c, and the threshold displacement energy, E_d. The parameters for aluminum were obtained from Konobeyev et al. [22] and those for copper and tungsten were obtained from Nordlund et al. [5].

Material	Aluminum	Copper	Tungsten
b	−1.00	−0.68	−0.56
c	0.44	0.16	0.12
E_d [eV]	27	33	70

3.1. Displacement cross section measurements

3.1.1. Proton beam fluence

A calibrated multi-wire chamber was placed in front of the sample to observe the intensity of the beam. The target chamber was placed on a moving stage that could be moved to within 0.1 mm. The beam profile at the sample position was measured by moving the stage horizontally by 1 mm and scanning the beam. Specifically, the electrical resistance of the tungsten wire at a temperature of 8 K was measured at each horizontal position for 20 min during irradiation with 120 GeV proton beams. The profile of the beam is fitted with a Gaussian distribution. The beam width induced in the wire (1 σ) was 5.74 ± 0.70 mm. Note that only horizontal beam scanning was carried out, as wires of 37.5 to 40 mm in length were attached vertically to the aluminum plate and variations of about mm in the vertical direction can be ignored. The vertical beam width at the sample location was adopted from the measurements of the multiwire chamber for beam scan as shown in Fig. 1.

The average fluence $\overline{\phi}$ is given by the following [9]:

$$\overline{\phi} = \frac{N_p}{2\pi\sigma_h\sigma_v LD} \int_{-D/2}^{D/2} exp\left(\frac{-x^2}{2\sigma_h^2}\right) dx \int_{-L/2}^{L/2} exp\left(\frac{-y^2}{2\sigma_v^2}\right) dy, \quad (9)$$

where x represents the horizontal position and y the vertical position. N_p is the integral number of protons in the incident beam, 6.43×10^{24}. L and D is the distance between two potentials and the diameter of a wire, respectively as indicated in Table 2. The damage rate is the ratio of the increase in resistivity to the average proton fluence along the sample line. The proton fluence was determined as follows. Half the length of the potential point (20 mm) is greater than the vertical beam width of σ_v (5.7 mm). Consequently, the integral value of the Gaussian to the vertical direction can be simplified to the following equation.

$$\frac{1}{\sqrt{2\pi}\sigma_v} \int_{-L/2}^{L/2} exp\left(\frac{-y^2}{2\sigma_v^2}\right) dy \cong 1, \quad (10)$$

Therefore, the averaged proton fluence, ϕ, is as follows.

$$\overline{\phi} = \frac{N_p}{\sqrt{2\pi}\sigma_h LD} \int_{-D/2}^{D/2} exp\left(\frac{-x^2}{2\sigma_h^2}\right) dx, \quad (11)$$

Finally, $\overline{\phi}$ is 1.12×10^{18}.

3.1.2. Damage rate

The motion table was moved horizontally to adjust the beam center position on the wire based on the beam scanning results before measuring the damage rate of the wire. Fig. 6 shows the time variation of the electrical resistance of the sample during the 120 GeV proton beam irradiation. The temperature was measured using a thermometer attached to the sample holder. The temperature was maintained at 8 K with the electrical heater during the proton beam irradiation.

Table 4 lists the increase of the electrical resistance, the electrical resistivity, and the damage rate. Those experimental errors are based on the electrical resistance measurements of all wires before the beam irradiation. The standard error of the damage rate is 22 % for aluminum, 4.8 % for copper, and 0.1 % for tungsten, respectively.

3.2. Displacement cross section

Table 4 also lists the experimental displacement cross-sections of wire samples obtained by **Eq. (1)**. Note that the error in Table 1 of the Frenkel pair resistivity changes is sufficiently large in comparison to the error in the damage rate for copper and tungsten. Therefore, it is dominant for the error in the displacement cross section. On the other hand, the error component of the damage rate for aluminum, 22 %, is

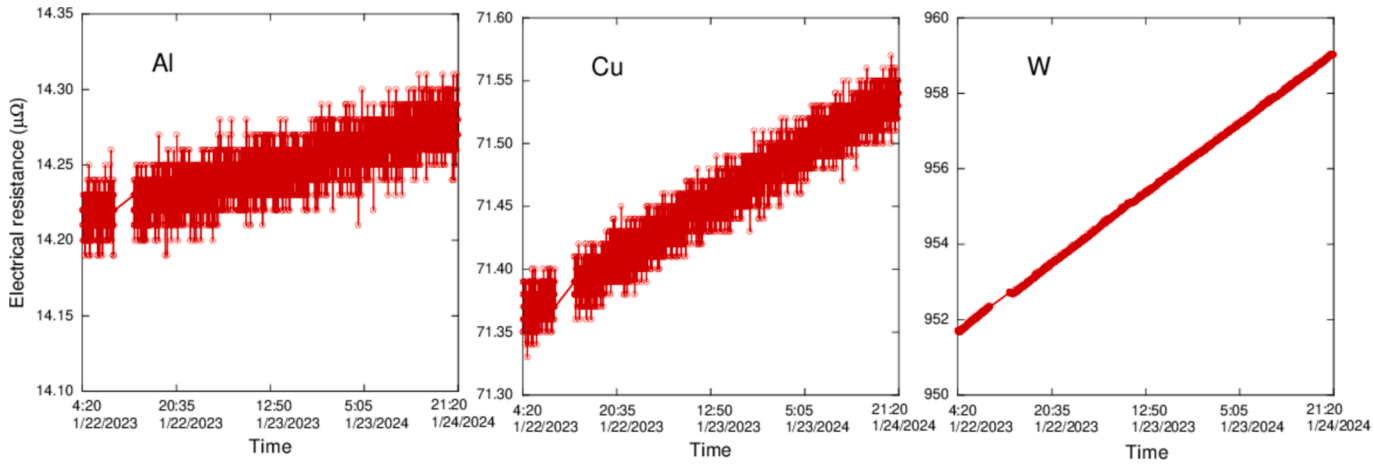

Fig. 6. Electrical resistance changes of aluminum, copper, and tungsten wires at 8 K during the 120-GeV proton irradiation.

Table 4
Results of the displacement damage of wire samples at 8 K under proton irradiation at 120 GeV.

Material	Aluminum	Copper	Tungsten
Electrical resistance increase, ΔR [Ω]	$(6.79 \pm 1.48) \times 10^{-8}$	$(1.65 \pm 0.08) \times 10^{-7}$	$(7.33 \pm 0.01) \times 10^{-6}$
Electrical resistivity increase, $\Delta\rho_0$ [Ωm]	$(8.33 \pm 1.82) \times 10^{-14}$	$(2.17 \pm 0.10) \times 10^{-13}$	$(9.59 \pm 0.01) \times 10^{-12}$
Damage rate, $\Delta\rho_m/\phi$ [Ωm^3/proton]	$(7.46 \pm 1.63) \times 10^{-32}$	$(1.82 \pm 0.09) \times 10^{-31}$	$(8.05 \pm 0.01) \times 10^{-30}$
Displacement cross section, $\sigma_{expt.}$ [barn]	202 ± 55	826 ± 192	2981 ± 662

also large for the error of displacement cross section.

Fig. 7 shows displacement cross sections of aluminum, copper and tungsten with protons. The dots indicate experimental data measured at the FTBF for 120 GeV proton (red points) and other facilities for low-energy protons of all targets [23], 185-MeV protons of aluminum and copper [7], 0.4–3 GeV protons of copper [9], 1.1 and 1.94-GeV protons of copper and tungsten [24], and 196-MeV protons of tungsten [8], respectively. The solid line shows the arc-dpa cross section and the dashed line shows the NRT dpa cross section calculated by PHITS, respectively. In all cases, the NRT-dpa cross sections are higher than the experimental data and the arc dpa cross sections are in close agreement with the experimental data over a wide range of proton energies. The displacement cross section decreases with proton energy below 20 MeV, depending on the Coulomb scattering cross section of the proton and target nucleus. Nuclear reaction products contribute more to the displacement cross section than incident protons in the proton energy region above 20 MeV.

3.3. Point defect recovery through annealing

When annealing irradiated metals, there is a stage at which defects disappear by diffusion into the sink or recombination, and a temperature range corresponding to this stage [25]. At cryogenic temperatures, electrical resistance measurements under irradiation are performed, where defects do not migrate. The duration of exposure determines the appearance of each stage. Therefore, there is no precise definition. Since the electrical resistivity is proportional to the total concentration of point defects induced by the irradiation, the damage rate is an indicator of the concentration of stable defects at a given temperature [25]. The electrical resistivity changes as a function of annealing temperature determine the defect reaction kinetics [25]. In this experiment, the isochronal holding times were set at 10 min for each annealing temperature. Fig. 8 shows defect concentration changes ($\Delta\rho/\Delta\rho_0$, where $\Delta\rho_0$ is an initial resistivity increase) to annealing temperature in metals after low temperature (below 10 K) irradiation. The left side of Fig. 8 has experimental data of copper irradiated with 120 GeV proton, 3 GeV proton [9], 196 MeV proton [7], 0.54 MeV proton [26], reactor neutron [27] and 1.3 MeV electron [28]. On the right are experimental data of tungsten irradiated with 120 GeV protons, 2.1 MeV electrons [29],

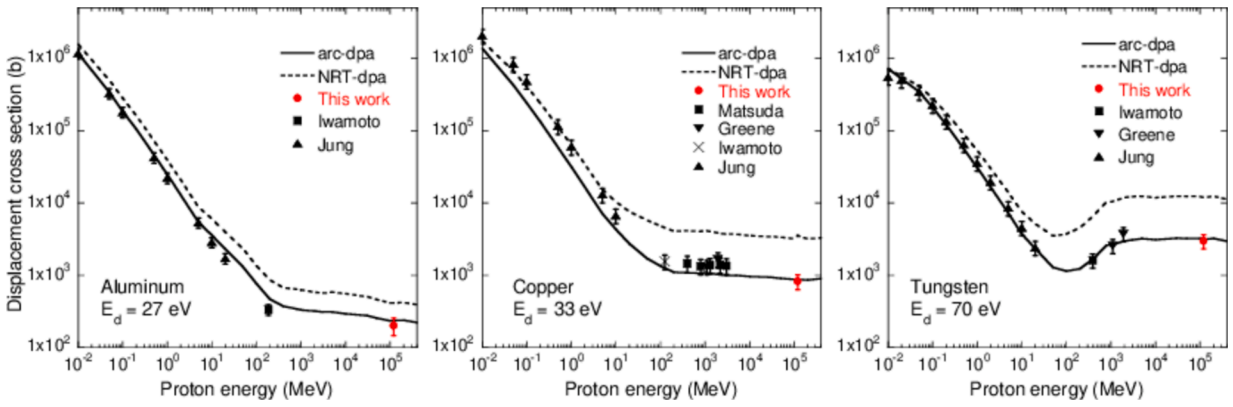

Fig. 7. Displacement cross sections of aluminum, copper and tungsten with proton. The dots indicate experimental data measured at the FTBF for 120 GeV proton (red points) and other facilities for low-energy protons of all targets [23], 185-MeV protons of aluminum and copper [7], 0.4–3 GeV protons of copper [9], 1.1 and 1.94-GeV protons of copper and tungsten [24], and 196-MeV protons of tungsten [8], respectively. (For interpretation of the references to colour in this figure legend, the reader is referred to the web version of this article.)

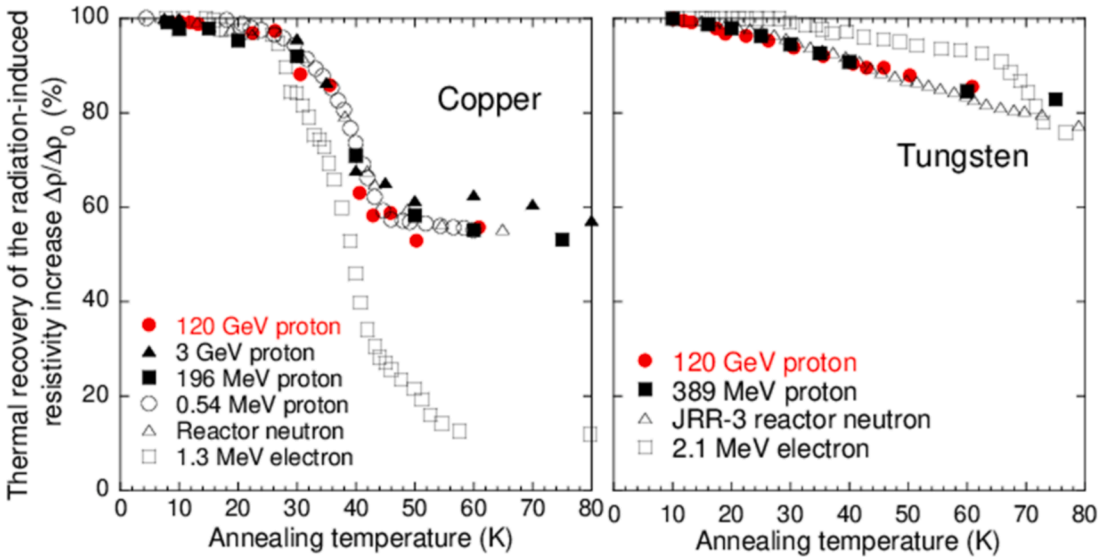

Fig. 8. Isochronal annealing curves of copper and tungsten samples irradiated at cryogenic temperature below 10 K.

reactor neutrons [30], and 389 MeV protons [8]. $\Delta\rho/\Delta\rho_0$ is the ratio of the amount of residual radiation defects to the initial amount of radiation defects. Note that due to the low $\Delta\rho_0$, 8.33×10^{-14} Ωm, for aluminum, the isochronal annealing curve for aluminum was not correctly obtained.

4. Discussion

Fig. 7 shows the calculated arc-dpa cross sections for 120 GeV protons agree with the experimental data within the error bars. The displacement cross sections of metals were nearly constant over the incident proton energy range from 1 GeV to 120 GeV. Yin et. al. [31] also reported the same tendency with their calculation at energies up to 100 GeV. As shown in Fig. 5, the damage energy increases proportionally to the PKA energy up to about 200 keV for aluminum, about 1 MeV for copper and about 10 MeV for tungsten. Beyond these PKA energies, the damage energy remains constant. At proton incident energies above 1 GeV, nuclear reaction products produced in the metal contribute to the damage and are considered as PKA in the calculations. Comparing the case of 1 GeV and 120 GeV proton incidence, the kinetic energy of the nuclear reaction products is sufficiently high and the energy loss due to elastic collisions is the same in both cases. The agreement between experimental data and calculated results at 120-GeV indicates that the displacement damage approximation proposed by Lindhard et al [22] is applicable to secondary particles produced by nuclear reactions.

Previous studies [16] have also shown that for proton energies above 1 GeV, the type and amount of nuclear reaction products depend on the proton energy, but the displacement cross section is constant. For example, when the proton incident energy is 1 GeV, the main nuclear reaction products are nuclides close to the proton number of the target, whereas when the proton incident energy is 50 GeV, a wide variety of nuclides with a wide range of proton numbers become nuclear reaction products and contribute to damage [16]. In terms of dpa index, proton incidence at 1 GeV and 120 GeV is almost the same, but the actual defect formation in the metal may be different. Both inelastic and elastic processes contribute to the overall damage, with the inelastic cross-section dominating the total cross section. Consequently, the simple displacement damage approximation may not accurately describe the damage at energies above 1 GeV. Additionally, secondary particles produced from primary collisions (p + p and p + n) further interact with the materials, causing additional damage. Future studies on the damage of materials to high-energy proton irradiation using other measurement methods, such as microscopy, are considered necessary.

In Fig. 8, the thermal recovery of metals under 120 GeV proton irradiation is almost the same as that of copper and tungsten irradiated with 196 MeV, 389 MeV and 3 GeV protons and reactor neutrons. This indicates that the damage densities of copper and tungsten caused by nuclear reaction products are the same in the high-energy proton and neutron irradiation environment, where nuclear reactions occur. It also shows that these damage densities are the same as those resulting from PKA due to elastic scattering of low-energy neutrons. In the case of copper, Stage I corresponds to the beginning of the self-interstitial migration of atoms [25] at temperatures below about 50 K. The recombination of vacancy-interlattice pairs, which were not placed far enough apart to escape attraction, occurs at low temperatures below about 30 K. [25]. As a result, the interlattice material recombines with the vacancies [25]. This suggests that the Frenkel pair density produced by neutrons and protons is higher than that of electrons, since the damage from proton and neutron irradiation remains about 55 %, while the damage from electron irradiation remains about 10 %. For tungsten, no different stages of thermal recovery are observed. About 80 % of the damage remains below 80 K. This indicates that tungsten has a higher damage density than copper. The defects are less easily recovered by heat, regardless of the energy of the incident particles.

5. Conclusion

To validate the dpa values for metals under 120 GeV proton beam irradiation, we measured the defect-induced changes in the electrical resistivity of wire of aluminum, copper and tungsten for proton irradiation with energies of 120 GeV at the FTBF. The experimental displacement cross sections were 202 ± 55 barn for aluminum, 826 ± 192 barn for copper, and 2981 ± 662 barn for tungsten, respectively. The results show that the NRT-dpa model of PHITS overestimates the experimental data, as the measurements for proton incidence below 3 GeV. On the other hand, the calculated results using the arc dpa model were in agreement with the measured displacement cross sections. The displacement cross sections are nearly constant above 1 GeV, because the damage energy of materials under 1 GeV proton irradiation is almost the same as that under 120 GeV proton irradiation. Measurements of damage recovery of accumulated defects in the sample by isochronal annealing as a function of defect concentration in the sample showed that approximately 60 % of the damage was recovered at 80 K for copper and 80 % for tungsten. The trend of damage recovery for 120 GeV protons was similar to the experimental results for other proton and neutron irradiations.

CRediT authorship contribution statement

Yosuke Iwamoto: Writing – review & editing, Writing – original draft, Visualization, Validation, Supervision, Project administration, Methodology, Investigation, Funding acquisition, Formal analysis, Data curation, Conceptualization. **Hiroki Matsuda:** Writing – review & editing, Software, Methodology, Investigation, Formal analysis, Data curation. **Shin-ichiro Meigo:** Writing – review & editing, Validation, Resources, Methodology, Investigation, Formal analysis, Data curation, Conceptualization. **Katsuya Yonehara:** Writing – review & editing, Resources, Methodology, Investigation, Funding acquisition, Conceptualization. **Frederique Pellemoine:** Writing – review & editing, Investigation. **Zunping Liu:** Writing – review & editing, Investigation. **Kevin Lynch:** Writing – review & editing, Investigation. **Makoto Yoshida:** Writing – review & editing, Software, Methodology. **Atsushi Yabuuchi:** Writing – review & editing, Software, Methodology. **Toshimasa Yoshiie:** Writing – review & editing, Resources. **Shintaro Hashimoto:** Writing – review & editing, Visualization.

Declaration of competing interest

The authors declare that they have no known competing financial interests or personal relationships that could have appeared to influence the work reported in this paper.

Acknowledgements

The authors wish to express their gratitude to Dr. N. Mokhov and the staff at FNAL for their generous support for planning this experiment and beam operation. They also wish to thank to Dr. T. Ishida, Dr. S. Makimura, and the staff at KEK and JAEA for their generous support for device development. This document was prepared with the support of RaDIATE collaboration using the resources of the KEK and Fermi National Accelerator Laboratory. This work is partially funded by the U.S.-Japan Science and Technology Cooperation Program in High Energy Physics. This manuscript has been authored by Fermi Research Alliance, LLC under Contract No. DE-AC02-07CH11359 with the U.S. Department of Energy, Office of Science, Office of High Energy Physics. This work is also supported by JSPS KAKENHI Grant Number JP16H04638 and JP19H02652.

Data availability

Data will be made available on request.

References

[1] https://j-parc.jp/c/en/index.html.
[2] https://www.fnal.gov/.
[3] https://home.cern/.
[4] M.J. Norgett, M.T. Robinson, I.M. Torrens, A proposed method of calculating displacement dose rates, Nucl. Eng. Des. 33 (1975) 50–54, https://doi.org/10.1016/0029-5493(75)90035-7.
[5] K. Nordlund, et al., Primary radiation damage: a review of current understanding and models, J. Nucl. Mater. 512 (2018) 450–479, https://doi.org/10.1016/j.jnucmat.2018.10.027.
[6] Y. Iwamoto, et al., Measurement of the displacement cross-section of copper irradiated with 125 MeV protons at 12 K, J. Nucl. Mater. 458 (2015) 369–375, https://doi.org/10.1016/j.jnucmat.2014.12.125.
[7] Y. Iwamoto, et al., Measurement of displacement cross sections of aluminum and copper at 5 K by using 200 MeV protons, J. Nucl. Mater. 508 (2018) 195–202, https://doi.org/10.1016/j.jnucmat.2018.05.038.
[8] Y. Iwamoto, et al., Measurements of displacement cross section of tungsten under 389-MeV proton irradiation and thermal damage recovery, Mater. Sci. Forum 1024 (2021) 95–101, https://doi.org/10.4028/www.scientific.net/MSF.1024.95.
[9] H. Matsuda, et al., Measurement of displacement cross-sections of copper and iron for proton with kinetic energies in the range 0.4-3 GeV, J. Nucl. Sci. Technol. 57 (2020) 1141–1151, https://doi.org/10.1080/00223131.2020.1771453.
[10] F. Pellemoine, The RaDIATE collaboration. https://radiate.fnal.gov/ (2023).
[11] https://ftbf.fnal.gov/.
[12] T. Sato, et al., Recent improvements of the Particle and Heavy Ion Transport code System - PHITS version 3.33, J. Nucl. Sci. Technol. 61 (2024) 127–135, https://doi.org/10.1080/00223131.2023.2275736.
[13] C.H.M. Broeders, A.Y. Konobeyev, Defect production efficiency in metals under neutron irradiation, J. Nucl. Mater. 328 (2004) 197–214, https://doi.org/10.1016/j.jnucmat.2004.05.002.
[14] A.V. Suslov, Stand alone experimental setup for dc transport measurements, Rev. Sci. Instruments 81 (2010) 075111, https://doi.org/10.1063/1.3463691.
[15] Y. Iwamoto, K. Niita, T. Sawai, R. Ronningen, T. Baumann, Improvement of radiation damage calculation in PHITS and tests for copper and tungsten irradiated with protons and heavy-ions over a wide energy range, Nucl. Instrum. Meth. B 55 (2012) 684–690, https://doi.org/10.1016/j.nimb.2011.11.038.
[16] Y. Iwamoto, S. Meigo, S. Hashimoto, Estimation of reliable displacements-per-atom based on athermal-recombination corrected model in radiation environments at nuclear fission, fusion, and accelerator facilities, J. Nucl. Mater. 538 (2020) 152261, https://doi.org/10.1016/j.jnucmat.2020.152261.
[17] A. Boudard, J. Cugnon, J. David, S. Leray, D. Mancusi, New potentialities of the liege intranuclear cascade model for reactions induced by nucleons and light charged particles, Phys. Rev. C 87 (2013) 014606, https://doi.org/10.1103/PhysRevC.87.014606.
[18] Y. Nara, H. Otuka, A. Ohnishi, K. Niita, S. Chiba, Relativistic nuclear collisions at 10A GeV energies from p+Be to Au+Au with the hadronic cascade model, Phys. ReV. C 61 (1999) 024901, https://doi.org/10.1103/PhysRevC.61.024901.
[19] S. Furihata, Statistical analysis of light fragment production from medium energy proton-induced reactions, Nucl. Instrum. Meth. B 171 (2000) 251–258, https://doi.org/10.1016/s0168-583x(00)00332-3.
[20] J. Lindhard, V. Nielsen, M. Scharff, P.V. Thomsen, Integral equations governing radiation effects (notes on atomic collisions, III), Mat. Fys. Medd. Dan. Vid. Selsk. 33 (1963).
[21] J., Lindhard, V. Nielsen, and M. Scharff, Approximation method in classical scattering by screened coulomb fields. Mat. Fys. Medd. Dan. Vid. Selsk. 36, 31p (1968).
[22] A.Y. Konobeyev, U. Fischer, Y.A. Korovin, S.P. Simakov, Evaluation of effective threshold displacement energies and other data required for the calculation of advanced atomic displacement cross-section, Nucl. Energy Technol. 3 (2017) 169–175, https://doi.org/10.1016/j.nucet.2017.08.
[23] P. Jung, Atomic displacement functions of cubic metals, J. Nucl. Mater. 117 (1983) 70–77, https://doi.org/10.1016/0022-3115(83)90011-9.
[24] G.A. Greene, Direct measurements of displacement cross sections in copper and tungsten under irradiation by 1.1-GeV and 1.94-GeV protons at 4.7 K, Proc. Sixth Int. Meet. on Nucl. Appl. Accel. Technol. (accapp03), San Diego. 881 (2003).
[25] G. Was, Fundamentals of radiation materials science, Springer-Verlag, New York, 2007.
[26] T. Iwata, A. Iwase, Damage production and annealing in ion-irradiated fcc metals, Radiat. Eff. Defects Solids 113 (1990) 135–154, https://doi.org/10.1080/10420159008213060.
[27] R.R. Coltman Jr., C.E. Klabunde, D.L. Mcdonald, J.K. Redman, Reactor damage in pure metals, J. Appl. Phys. 33 (1962) 3509–3522, https://doi.org/10.1063/1.1702438.
[28] J.W. Corbett, J.M. Denney, M.D. Fiske, R.M. Walker, Electron irradiation of copper near 10 K, Phys Rev. 108 (1957) 954–964, https://doi.org/10.1103/PhysRev.108.954.
[29] H. H. Neely, D.W. Keefer and A. Sosin, Electron irradiation and recovery of tungsten. Phys. Stat. Sol. 28 (1968) 675–582, DOI: https://doi.org/10.1002/pssb.19680280225.
[30] S. Takamura, R. Hanada, S. Okuda, H. Kimura, Recovery of low-temperature fast neutron irradiated tungsten, J. Phys. Soc. Jpn. 30 (1971) 1091–1095, https://doi.org/10.1143/JPSJ.30.1091.
[31] W. Yin, A. Konobeyev, D. Leichtle, L. Cao, Calculation of displacement damage cross-section for charged particles at energies up to 100 GeV, J. Nucl. Mater. 573 (2023) 154143, https://doi.org/10.1016/j.jnucmat.2022.154143.